Fortuin-Kasteleyn and damage-spreading transitions in random-bond Ising lattices

P. H. Lundow[1] and I. A. Campbell[2]
[1]*Department of Theoretical Physics, Kungliga Tekniska högskolan, SE-106 91 Stockholm, Sweden*
[2]*Laboratoire Charles Coulomb, Université Montpellier II, 34095 Montpellier, France*
(Received 1 May 2012; revised manuscript received 10 July 2012; published 12 October 2012)

The Fortuin-Kasteleyn and heat-bath damage-spreading temperatures $T_{\rm FK}(p)$ and $T_{\rm DS}(p)$ are studied on random-bond Ising models of dimensions 2–5 and as functions of the ferromagnetic interaction probability p; the conjecture that $T_{\rm DS}(p) \sim T_{\rm FK}(p)$ is tested. It follows from a statement by Nishimori that in any such system, exact coordinates can be given for the intersection point between the Fortuin-Kasteleyn $T_{\rm FK}(p)$ transition line and the Nishimori line $[p_{\rm NL,FK}, T_{\rm NL,FK}]$. There are no finite-size corrections for this intersection point. In dimension 3, at the intersection concentration $[p_{\rm NL,FK}]$, the damage spreading $T_{\rm DS}(p)$ is found to be equal to $T_{\rm FK}(p)$ to within 0.1%. For the other dimensions, however, $T_{\rm DS}(p)$ is observed to be systematically a few percent lower than $T_{\rm FK}(p)$.

DOI: 10.1103/PhysRevE.86.041121 PACS number(s): 05.50.+q, 75.50.Lk, 64.60.Cn, 75.40.Cx

I. INTRODUCTION

The physics of Ising spin glasses (ISGs) in the ordered regime below the freezing temperature T_g has been intensively investigated for decades; the paramagnetic regime above T_g has attracted less attention. However, in addition to the standard ordering (or freezing) transitions, other significant critical temperatures within the paramagnetic regime can be defined operationally and estimated numerically with high precision.

We have studied random-bond Ising models (RBIMs) in dimensions 2–5 having ferromagnetic near-neighbor interactions with probability p and antiferromagnetic interactions with probability $1-p$ over the whole range of p in the paramagnetic regime. The Hamiltonian is $H = \sum_{ij} -J_{ij} S_i S_j$, where the sum is taken over all nearest-neighbor bonds ij.

For the discrete $\pm J$ interaction distribution the bond values are thus chosen according to

$$P(J_{ij}) = p\delta(J_{ij} - J) + (1-p)\delta(J_{ij} + J). \qquad (1)$$

We will set $J = 1$ and use when convenient inverse temperatures $\beta = 1/T$. The pure Ising model is recovered for $p = 1$ and the pure antiferromagnetic model for $p = 0$, while the standard strong-disorder bimodal spin glass case corresponds to $p = 1/2$.

In addition to the standard ferromagnetic and spin glass ordering transitions, on the RBIM phase diagram in the paramagnetic regime other physically significant lines can be operationally defined as functions of p. In addition to the Griffiths line $T_{\rm Gr}(p) = T_c$ [1,2] and the Nishimori line [3] there is the Fortuin-Kasteleyn (FK) transition line $T_{\rm FK}(p)$ [4–9] and the heat-bath damage-spreading transition line $T_{\rm DS}(p)$ [10–13]. Early large-scale relaxation measurements on the ISG in dimension 3 were interpreted [14] in terms of a dynamic transition at the Griffiths temperature [i.e., $T_G(p) = T_c$], with a qualitative change in relaxation behavior of the autocorrelation function from nonexponential to exponential.

It can alternatively be considered that $T_{\rm FK}$ or $T_{\rm DS}$ defines a dynamic transition. At $T_{\rm FK}$ the FK cluster size diverges so the standard cluster flipping algorithms [15,16] break down. At $T_{\rm DS}$, the time scale for the coupling from the past equilibration criterion $D(t) \to 0$ diverges at large L [17,18], so this criterion similarly breaks down. *A priori* it seems plausible that the two dynamic breakdowns should occur at similar, if perhaps not identical, temperatures, as has been conjectured by a number of authors [7,19,20].

In the following discussion it is shown that there are universal analytic relations for the intersection point between $T_{\rm FK}(p)$ and the Nishimori line [3]. With these exact values in hand together with the present accurate numerical damage-spreading data a critical test can be made of the conjectured rule $T_{\rm DS}(p) \sim T_{\rm FK}(p)$. This is shown to be a good approximation, almost exact in dimension 3 and accurate to a few percent in dimensions 2, 4, and 5. However the equality between the temperatures is not a general rule.

II. TRANSITION DEFINITIONS

Nishimori [3] has shown for the RBIM that, due to extra symmetries of the problem, a number of quantities may be computed exactly when the equality

$$(1 - p_{\rm NL})/p_{\rm NL} = \exp(-2\beta_{\rm NL}) \qquad (2)$$

holds; this condition defines the Nishimori line (NL), a line traversing the entire $\beta(p)$ phase diagram including both paramagnetic and ferromagnetic regimes. In particular on the NL the internal energy of the system per bond (or edge) is

$$U_{\rm NL} = -[2p_{\rm NL} - 1] = -\tanh(\beta_{\rm NL}). \qquad (3)$$

This energy per bond has exactly the value that independent bonds would have at the same temperature. We will see below that indeed on the NL the positions of the satisfied bonds are uncorrelated [21,22] and that bond positions remain very close to random over a wide strong-disorder regime around $p = 1/2$. In other words, anywhere on the NL the satisfied bonds are uncorrelated on average, so *a fortiori* the FK active bonds are distributed at random.

The rule for the FK transition line [4–9], corresponding initially to the pure ferromagnets, is to first select for some particular equilibrium configuration the entire set of satisfied bonds ij where $J_{ij} S_i S_j$ is positive. These bonds are then decimated at random, leaving a fraction $[1 - \exp(-2/T)]$ of active satisfied bonds. The FK stochastic transition at $T_{\rm FK}$ occurs when the set of active bonds percolates through the

lattice. From the way in which the bonds are laid down, in the general case this is correlated bond percolation, as opposed to the standard uncorrelated bond percolation with random-bond occupation. Remarkably, for pure ferromagnets it can be proved that the FK transition $\beta_{\rm FK}(p=1)$ coincides exactly with the Curie temperature $\beta_c(p=1)$ [4]. The Swendsen-Wang and Wolff cluster algorithms [15,16] speed up equilibration dramatically as long as the FK clusters remain of finite size.

The same operational definition can also be used elsewhere in the phase diagram; in particular $T_{\rm FK}(p=1/2)$ was estimated numerically for strong-disorder RBIM on square, cubic, and triangular lattices [6–9]. It turned out that $T_{\rm FK}(p=1/2)$ was in each case much higher than the standard spin glass ordering temperature $T_g(p=1/2)$. Even in the two-dimensional case where the glass temperature is zero, $T_{\rm FK}(p=1/2)$ is similar to but lower than the Griffiths temperature $T_{\rm Gr}=T_c(p=1)$ [8,9]. The physical basis for the percolation transition temperature was explained in terms of FK droplets for the case of the fully frustrated lattice and general Potts q in Refs. [23,24]. Imaoka *et al.* [25] estimated $T_{\rm FK}(p)$ numerically over the entire range of p for the square and triangular RBIM lattices.

Below we will introduce a further temperature $T_{{\rm FK}r}(p)$ closely related to $T_{\rm FK}(p)$. By construction the fraction of satisfied bonds $n_s(p,T)$ in equilibrium is related to the equilibrium internal energy per bond $U(p,T)$ through $U(p,T)=1-2n_s(p,T)$, so the fraction of all bonds that are FK active bonds is just [19]

$$P_a(p,T)=[1-U(p,T)][1-\exp(-2/T)]/2. \qquad (4)$$

The $U(p,T)$ and hence $P_a(p,T)$ can be readily measured numerically to high precision. It was noted [19] that if the satisfied bond positions are assumed to be uncorrelated, the FK transition would occur at a temperature such that $P_a(p,T_{\rm FK})\equiv P_c$, where P_c is the standard random-bond percolation concentration for the lattice.

We will refer to the temperature where the condition

$$P_a(p,T_{{\rm FK}r})=P_c \qquad (5)$$

is satisfied as $T_{{\rm FK}r}(p)$ (r standing for random). This conjecture led to estimates for $T_{{\rm FK}r}(p=1/2)$ on square and cubic lattices in higher dimensions [19] that were in good agreement with the numerical estimates for $T_{\rm FK}(p=1/2)$ available at the time.

It can be noticed that for the pure Ising square lattice ferromagnet at criticality $U(\beta_c)=-1/2^{1/2}=-0.7071\ldots$, while $-\tanh(\beta_c)=-0.4121\ldots$, which is very different because the positions of the satisfied bonds are strongly correlated. However, the critical FK concentration of active bonds is $P_a(p=1,T_c)=1/2$, which is unintentionally equal to $P_c=1/2$ for this lattice. For the pure Ising ferromagnet on the triangular lattice at criticality, in contrast, $P_a(p=1,T_c)=0.352\,208\ldots$, which is not quite equal to $P_c=0.347\,296\ldots$ for this lattice.

Finally, a heat-bath damage-spreading transition $T_{\rm DS}(p)$ can be defined [10–13]. Heat-bath update rules are applied at fixed temperature to two initially nonidentical spin configurations $A(0)$ and $B(0)$ (which are not necessarily equilibrated) of a given sample (meaning A and B have exactly the same sets of interactions J_{ij}); the random number used in each subsequent single spin update step is the same for both configurations. At high enough temperatures, on annealing under this procedure for sufficient time t, $A(t)$ and $B(t)$ will become identical; below the damage temperature $T_{\rm DS}$ the damage [$D(t)$ is the Hamming distance between $A(t)$ and $B(t)$ divided by L^d] will stabilize for long times at a temperature-dependent nonzero value. For the pure ferromagnetic case $T_{\rm DS}(p=1)$ is equal to the Curie temperature $T_c(p=1)$ [10,11]. For the strong-disorder spin glass, just as $T_{\rm FK}(p=1/2)$ is much higher than the glass temperature $T_g(p=1/2)$, $T_{\rm DS}(p=1/2)$ is also much higher than $T_g(p=1/2)$ [10–13]. The damage-spreading transition for a given coupling algorithm, in particular the heat bath (HB), can be described as a regular to chaotic dynamic transition from the viewpoint of the coupling from the past approach. When the damage falls to zero after a sufficient anneal time it is a guarantee that the system has been strictly equilibrated [18,26,27]. In systems with frustration this guarantee breaks down when $T<T_{\rm DS}(p)$, so perfect equilibration in this sense for the regime near the critical temperature cannot be achieved.

It should be noted that $T_{\rm DS}$ depends on the updating protocol, with, for instance, Glauber updating giving very different results from HB updating. It turns out that even within the HB protocol the precise value obtained for $T_{\rm DS}$ changes slightly depending on whether sequential or random updating is used. The results reported here are for random updating. With sequential updating the observed damage-spreading temperature is of the order of 1% lower.

Early comparisons of numerical data from different groups indicated that $T_{\rm DS}(p=1/2)\sim T_{\rm FK}(p=1/2)$ for dimensions 2 and 3 [7,19] and on this basis it has been conjectured by a number of authors [7,19,20] that $T_{\rm DS}(p)\sim T_{\rm FK}(p)$ is a general rule defining a joint dynamic transition temperature above which relaxation is exponential in the long-time limit and below which relaxation is chaotic. It should be noted that in practice it is very hard to identify such a transition directly from autocorrelation function decay $q(t)$ data.

Recently Yamaguchi [20] focused attention on the behavior on the NL. He provided conjectures suggesting that the intersection of the $T_{\rm FK}(p)$ line and the NL would occur when

$$p_{\rm NL,FK}=(1+P_c)/2 \qquad (6)$$

and

$$\beta_{\rm NL,FK}=\ln[(1+P_c)/(1-P_c)]/2, \qquad (7)$$

where again P_c is the random percolation concentration for the lattice. It turns out that because of the analytic value for the energy $U_{\rm NL}(p)$ on the NL [Eq. (3)], the Yamaguchi condition is strictly equivalent to the equality $T_{\rm NL,FK}=T_{{\rm NL,FK}r}$, meaning that this condition holds if the FK active bonds are distributed at random. The random-bond conjecture for $\beta_{\rm FK}$ [Eq. (4) of Ref. [19]] is identical to Eq. (3.3) of Ref. [20].

In fact, Nishimori [21] years earlier had made the following strict statement: "We have also proved independence of the local internal energy of different bonds, which indicates that the system effectively splits into uncorrelated sets of bonds on the [NL] in the phase diagram." In other words, anywhere on the NL the satisfied bonds are uncorrelated *on average*, so *a fortiori* the FK active bonds are distributed at random. Hence, at the NL-FK intersection concentration $p_{\rm NL,FK}$, we have $T_{\rm FK}\equiv T_{{\rm FK}r}(p)$, meaning that the conditions for this

intersection conjectured by Yamaguchi [Eqs. (6) and (7)] hold exactly for any RBIM lattice if the FK transition is a random active-bond percolation transition. Remarkably, a further consequence of Nishimori's statement is that this equality should hold *for the mean over many samples* independently of the sample size L.

The numerical results below show that for dimension 2, and presumably in other dimensions also, in addition to this identity at $p_{\mathrm{NL,FK}}$, for a wide range of p around $p = 1/2$, $T_{\mathrm{FK}}(p) \sim T_{\mathrm{FK}r}(p)$ remains a very good approximation, as was conjectured for $p = 1/2$ in Ref. [19]. The active bonds are thus essentially uncorrelated at $\beta_{\mathrm{FK}}(p)$ in this wide high-disorder regime. It should be noted, however, that as a general rule, the positions of active bonds are correlated so $T_{\mathrm{FK}}(p)$ is not equal to $T_{\mathrm{FK}r}(p)$.

Yamaguchi [20], following Refs. [7,19] for the case of $p = 1/2$, also conjectured that $T_{\mathrm{DS}}(NL) = T_{\mathrm{NL,FK}}$ at the intersection. The present measurements show that in dimension 2, $T_{\mathrm{DS}}(p)$ is in fact systematically lower than $T_{\mathrm{FK}}(p)$ by a few percent over the entire range of p, except at and near the pure ferromagnet limit $p = 1$. At $p_{\mathrm{NL,FK}}$ for cubic models in dimensions 3–5 the conjecture holds to within about 0.1% in dimension 3, to 2% in dimension 4, and to 4% in dimension 5. The general relation $T_{\mathrm{DS}}(p) \sim T_{\mathrm{FK}}(p)$ is therefore simply a reasonably good approximation. In dimensions 2–4 the present data show that the damage-spreading transition temperature, like the FK transition temperature, is very insensitive to p for a wide range of p around $p = 1/2$.

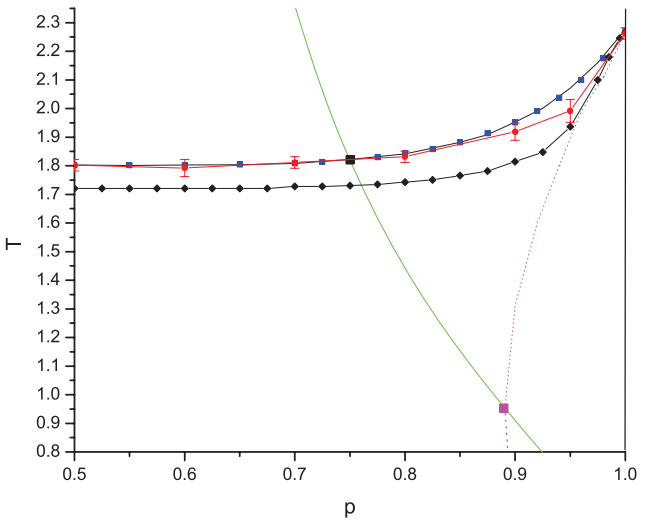

FIG. 1. (Color online) Square lattice transitions. Temperatures T are shown as functions of the ferromagnetic interaction concentrations p. The pink dashed line on the right indicates the ferromagnetic Curie temperatures; the data are taken from Ref. [32]. The green solid traversal line is the exact Nishimori line. Red circles denote the FK transitions T_{FK}, from Ref. [25]. Blue squares denote the random active-bond percolation line $T_{\mathrm{FK}r}$. Black diamonds denote the heat-bath damage-spreading transition T_{DS}. The errors on T_{FK} and T_{DS} are the size of the points. The large black square is the exact intersection point $T_{\mathrm{NL,FK}}$.

III. FORTUIN-KASTELEYN NUMERICAL RESULTS IN DIMENSION 2

The two-dimensional lattices studied were the square lattice and the triangular lattice. On both lattices the standard phase diagrams as functions of p are well established. The pure ferromagnetic Curie temperatures $T_c(p = 1)$ are exactly $T_c(\mathrm{sq}) = -2/\ln[2^{1/2} - 1] = 2.269\,18\ldots$ and $T_c(\mathrm{tri}) = 4/\ln 3 = 3.640\,96\ldots$, respectively. When p is lowered from $p = 1$, the Curie temperature $T_c(p)$ drops gradually until a critical point is reached at p_r on the Nishimori line, where the Curie temperature tends suddenly to zero with weak re-entrant behavior [3,28–32]. Between the re-entrant regime and $p = 1/2$ the system can be considered a spin glass, but with no finite-temperature ordering transition. The square lattice phase diagram for $p < 1/2$ is the exact mirror image of the phase diagram for $p > 1/2$, with antiferromagnetic order taking the place of ferromagnetic order as the lattice is bipartite. For the triangular lattice, in contrast, there is no finite-temperature order below $p = 1/2$ as the fully frustrated antiferromagnetic limit at $p = 0$ is approached.

The internal energy per bond $U(p,T,L)$ at equilibrium was estimated numerically. For small triangular lattices $3 \leqslant L \leqslant 11$, the energy as a function of temperature for each specific sample was calculated exactly (up to numerical precision) using transfer matrices. Once a sample is picked we split the lattice into L parts, each part corresponding to a transfer matrix A_i. After choosing a numerical value of T we evaluate the matrices and compute the trace of their product to obtain $Z(p,T,L) = \mathrm{tr}(A_1\, A_2 \cdots A_L)$. This standard approach is described in great detail for the Ising case in Sec 3 of Ref. [33] and is of course easily adapted to the spin glass case. We thus computed $\langle \ln Z(p,T,L)\rangle$ for $p = 0,0.02,0.04,\ldots,0.50$ and $p = 0.51,\ldots,0.98,0.99,1$ and some 70–80 values of T. The number of samples ranged between 16 384 for $L = 3,4,5$ and then down to only 1024 for $L = 11$. Taking the average $\partial \ln Z/\partial\beta$ then provides us with $\langle U(p,T,L)\rangle$. Values at (p,T) outside the computed data grid were obtained through third-order interpolation.

For larger L (for the square and triangular lattices) the Monte Carlo data were collected after equilibration using standard Metropolis updating. At each (p,T), and for each sample, we collected at least a few 10^6 measurements of U and of course even more for moderate L. For the square lattices we used $L = 16,32,64$ on 64 different samples with $0.5 \leqslant p < 1$ in steps of 0.025. For the triangular lattice we used $L = 16,32$ on 32 different samples but with $0 < p < 1$ in steps of 0.025 (slightly denser at high and low p). Some 50 values of T were used for both lattices. Again, intermediate values of $\langle U\rangle$ were obtained by interpolating the values at the (p,T) grid points. By interpolation of points derived from Eq. (4) and the consistency condition (5) the temperature $T_{\mathrm{FK}r}(p)$ where the fraction of FK active bonds $P_a(p,T)$ is equal to P_c can be estimated to high precision. In Figs. 1 and 2 the $T_{\mathrm{FK}r}(p)$ values are compared to the directly measured $T_{\mathrm{FK}}(p)$ values [8,25] for the square and triangular lattices, respectively. The damage-spreading temperatures to be discussed later are also shown.

The error in the $T_{\mathrm{FK}r}$ estimates is found by first solving Eq. (4) for each individual sample (using the interpolation we mentioned above), which gives us a sample-to-sample standard deviation from which we obtain the standard error of the

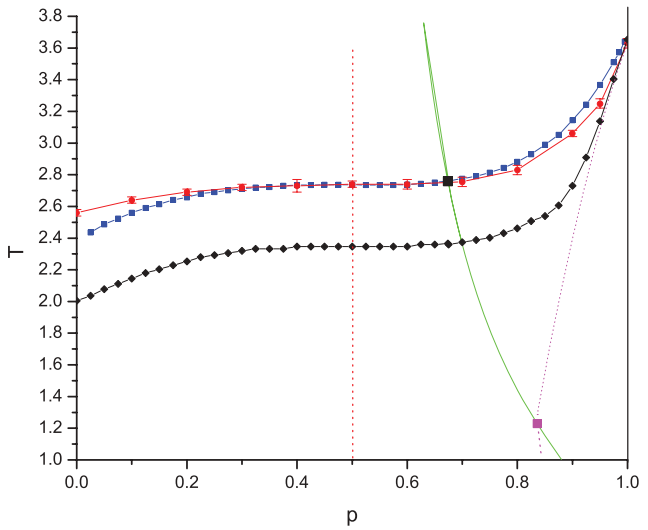

FIG. 2. (Color online) Triangular lattice transitions. Temperatures T are shown as functions of the ferromagnetic interaction concentrations p. The pink dashed line on the right indicates the ferromagnetic Curie temperatures. The green solid traversal line is the exact Nishimori line. The red dashed vertical line in the center indicates $p = 0.5$. Red circles denote the FK transitions $T_{\rm FK}$, from Ref. [25]. Blue squares denote the random active-bond percolation line $T_{{\rm FK}r}$. Black diamonds denote the heat-bath damage-spreading transition $T_{\rm DS}$. The errors on $T_{\rm FK}$ and $T_{\rm DS}$ are the size of the points. The large black square is the exact intersection point $T_{\rm NL,FK}$.

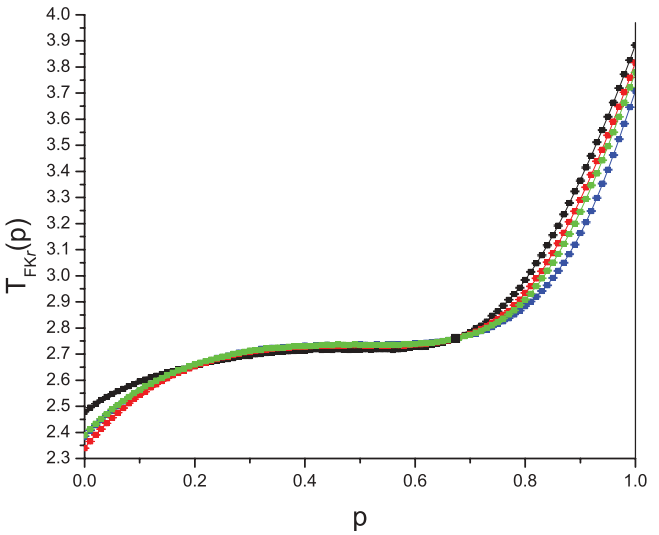

FIG. 3. (Color online) Size effect on triangular lattice temperatures $T_{{\rm FK}r}$ at which the fraction of FK sites is equal to the random site percolation concentration for the lattice P_c [Eq. (5)]. Temperatures $T_{{\rm FK}r}$ are shown as functions of the ferromagnetic interaction concentrations p for lattice sizes L from 3 to 11: $L = 3$, 4, 5, and 11 are indicated by black, red, green, and blue, respectively, from top to bottom on the right-hand side and from bottom to top on the left-hand side. The black square is the exact $T_{\rm NL,FK}$ intersection [Eqs. (6) and (7)].

average sample $T_{{\rm FK}r}$. Once the standard error is established we are free to plot a smoothed version (from fitting a polynomial of high degree) of $T_{{\rm FK}r}$ versus p. Needless to say, we have not estimated the error in U, and hence $T_{{\rm FK}r}$, for each individual sample, but we simply assume this error should be reflected in the sample-to-sample variation.

In dimension 2, $P_c = 1/2$ for the square lattice and $P_c = 2\sin(\pi/18) = 0.347\,296\,355\ldots$ for the triangular lattice. The exact NL-FK intersection values from Eqs. (6) and (7) are then $p_{\rm NL,FK} = 3/4$ and $\beta_{\rm NL,FK} = \ln(3)/2 = 0.549\,306\,3\ldots$ for the square lattice and $p_{\rm NL,FK} = 0.6736\ldots$ and $\beta_{\rm NL,FK} = 0.362\,371\ldots$ for the triangular lattice. The estimated $T_{\rm FK}(p)$ and $T_{{\rm FK}r}(p)$ lines run directly through these exact NL-FK intersection points as they should (Figs. 1 and 2).

The measured equilibrium energy per bond is slightly higher than the random-bond energy $-\tanh(\beta)$ for $\beta > \beta_{{\rm FK}r}$ and slightly lower for $\beta < \beta_{{\rm FK}r}$. To within the high numerical precision the estimated $\beta_{{\rm FK}r}(p_{\rm NL,FK}, L)$ at the NL-FK intersection point is independent of L down to $L = 3$ (Figs. 3 and 4). The observed absence of finite scaling corrections at the NL also follows from Nishimori's general statement quoted above [21]. For p values to the left and right of $p_{\rm NL,FK}$ there are weak finite-size effects of opposite signs. This absence of mean finite-size scaling deviations arises because $T_{{\rm FK}r}$ depends only on the energy. Other parameters can still show finite-size scaling deviations [34]. The large-size limits for $T_{\rm FK}(p)$ and $T_{{\rm FK}r}(p)$ remain equal to each other to within the numerical precision of the $T_{\rm FK}(p)$ points [25] over the strong-disorder range of p extending from $p = 1/2$ to $p_{\rm NL,FK}$ in the square lattice and from $p \sim 0.3$ to $p_{\rm NL,FK}$ in the triangular lattice. Over these ranges of p the satisfied bonds at $T_{\rm FK}$ are very close to being uncorrelated; for instance, at $p = 1/2$ on the square lattice $-U(p,\beta_{{\rm FK}r})/\tanh(\beta_{{\rm FK}r}) = 0.9709$, which remains close to the uncorrelated value of 1. The further

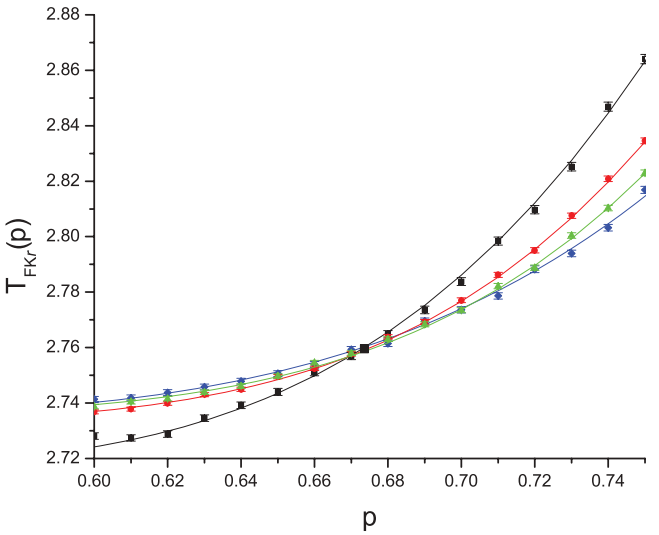

FIG. 4. (Color online) Same as for Fig. 3: a closeup of the region around the $T_{\rm NL,FK}$ intersection (large black square). Here $L = 3$, 4, 5, and 11 are shown as black squares, red circles, green triangles, and blue diamonds, respectively, from top to bottom on the right-hand side and from bottom to top on the left-hand side). The error bars are the standard error when measuring $T_{{\rm FK}r}$ after solving Eqs. (4) and (5) and correspond to 16 384 samples for $L = 3$,4,5 and 1024 samples for $L = 11$. The curves are tenth-degree polynomials fitted to the whole range from $p = 0$ to 1.

randomness introduced by the FK decimation is sufficient to render the active-bond positions essentially uncorrelated. The $T_{\mathrm{FK}}(p)$ [25] [or $T_{\mathrm{FK}r}(p)$, which has been measured here with higher precision] is rather insensitive to p within this range, so the measured $T_{\mathrm{FK}}(1/2)$ is similar to the exact $T_{\mathrm{NL,FK}}$ on both lattices. For both lattices in the more strongly ferromagnetic ranges $p > p_{\mathrm{NL,FK}}$ and in the range $p < 0.3$ close to the fully frustrated $p = 0$ limit in the triangular lattice, $T_{\mathrm{FK}}(p) > T_{\mathrm{FK}r}(p)$. At these concentrations the satisfied bonds are significantly correlated at $T_{\mathrm{FK}}(p)$ and the FK decimation does not sufficiently compensate for the correlations so as to produce randomness among the active bonds.

IV. DAMAGE-SPREADING NUMERICAL RESULTS IN DIMENSION 2

For dimension 2 the critical temperatures $T_{\mathrm{DS}}(p)$ below which the long-time large-L heat-bath damage spreading $D(p,T,t)$ tends to a nonzero value are also shown in Figs. 1 and 2. The values given are obtained from extrapolating data at increasing sizes (Figs. 5 and 6) to infinite size. On the basis of data for square and cubic lattices at $p = 1/2$ it was conjectured earlier that $T_{\mathrm{FK}}(p) \sim T_{\mathrm{DS}}(p)$ [7,19,20], as is the case in the pure ferromagnetic $p = 1$ limit. However, the present data demonstrate that while the curves for $T_{\mathrm{DS}}(p)$ and $T_{\mathrm{FK}}(p)$ lie close together and are of very similar shape, in particular both being almost independent of p for the range near $p = 1/2$, it is clear that $T_{\mathrm{DS}}(p) < T_{\mathrm{FK}}(p)$ except when p tends to the ferromagnetic limit $p = 1$. Thus, unfortunately, it is not possible to define a unique joint dynamic transition temperature. We will see that this is true also in higher dimensions.

The present accurate critical value for the strong-disorder square lattice $T_{\mathrm{DS}}(1/2) = 1.69(2)$ is in good agreement with the earlier value $T_{\mathrm{DS}}(1/2) = 1.70$ [13] and is very close to the regular to chaotic dynamic transition temperature estimated for the same lattice in Ref. [18] from the divergence of the coupling time with L^2, where the data indicate a transition at $T_{\mathrm{DS}}(1/2) \sim 1.72$.

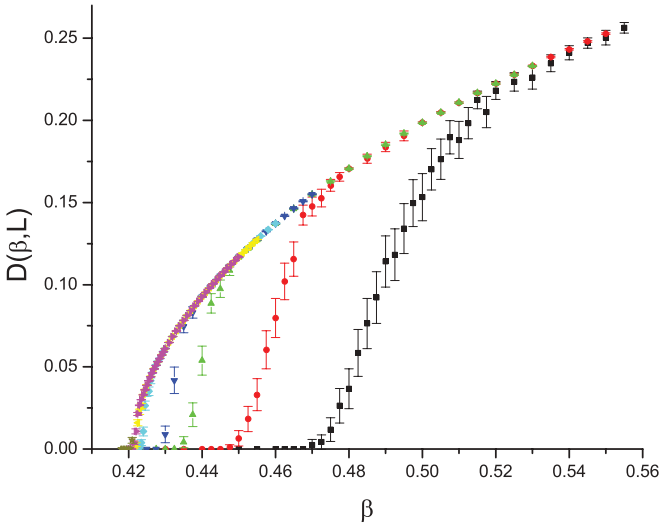

FIG. 5. (Color online) Damage spreading $D(\beta,L)$ for the triangular lattice at $p = 0.6736$. The lattice sizes are $L =$ 48, 64, 96, 128, 256, 384, 512, and 1024 are shown as black squares, red circles, green triangles, blue inverted triangles, cyan diamonds, yellow left-pointing triangles, pink right-pointing triangles, and brown stars, respectively, from right to left in the region where the curves separate. Shown error bars are the standard error. The exact FK transition inverse temperature is $\beta = 0.362\,371\ldots$, which is distinct from the limiting damage-spreading inverse temperature.

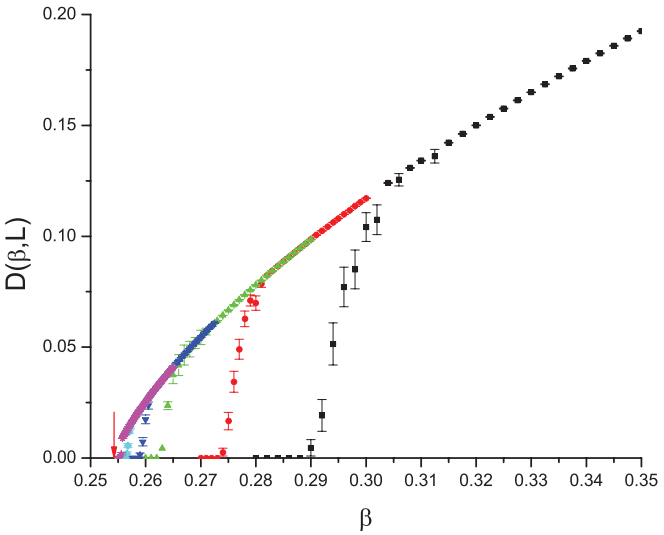

FIG. 6. (Color online) Cubic lattice equilibrium damage spreading $D(\beta,L)$ as a function of size and inverse temperature for $p = 0.6244$. The sizes $L = 12$, 16, 24, 32, 48, and 64 are shown as black squares, red circles, blue triangles, green inverted triangles, cyan diamonds, and pink stars, respectively, from right to left in the region where the curves separate. Shown error bars are the standard error. The extrapolated intersection with the β axis gives the infinite-size critical β_{DS}. In this case $\beta_{\mathrm{DS}} = 0.254\,32(15)$ can hardly be distinguished from the exact FK transition inverse temperature $\beta_{\mathrm{FK}} = 0.254\,14\ldots$ (red arrow).

V. DIMENSIONS 3–5

It is numerically much more demanding to estimate $T_{\mathrm{FK}}(p)$ precisely through direct measurements (as in Ref. [25]), in particular allowing for finite-size effects, than to estimate $T_{\mathrm{DS}}(p)$ to the same level of accuracy. For cubic lattices in dimensions 3, 4, and 5 the random-bond critical concentrations P_c, though not exact, have been estimated to very high precision: $P_c(3) = 0.248\,812\,6(5)$, $P_c(4) = 0.160\,131\,0(10)$, and $P_c(5) = 0.118\,117\,18(3)$, respectively [35,36]. Using the exact NL-FK intersection point expressions (6) and (7), one thus has $p_{\mathrm{NL,FK}} = 0.6244$ and $\beta_{\mathrm{NL,FK}} = 0.254\,146\,6$ in dimension 3, $p_{\mathrm{NL,FK}} = 0.580\,06$ and $\beta_{\mathrm{NL,FK}} = 0.161\,521$ in dimension 4, and $p_{\mathrm{NL,FK}} = 0.559\,06$ and $\beta_{\mathrm{NL,FK}} = 0.118\,671$ in dimension 5. Hence, as $p_{\mathrm{NL,FK}}$ and $\beta_{\mathrm{FK}}(p_{\mathrm{NL,FK}})$ can be taken as known almost exactly, it is sufficient to estimate $\beta_{\mathrm{DS}}(p_{\mathrm{NL,FK}})$ numerically (allowing carefully for finite-size corrections) to obtain an accurate estimate of the ratio $T_{\mathrm{DS}}(p_{\mathrm{NL,FK}})/T_{\mathrm{FK}}(p_{\mathrm{NL,FK}})$ for each dimension.

The equilibrium damage $D(L,\beta)$ was measured for given L as a function of β and the results were extrapolated to obtain an estimate of the β_{DS} value at which $D(\infty,\beta)$ falls to zero (Figs. 5 and 6). There is a clear envelope curve for all L in each case, with the data points leaving the curve later and later as L increases. There are various ways to extrapolate to infinite

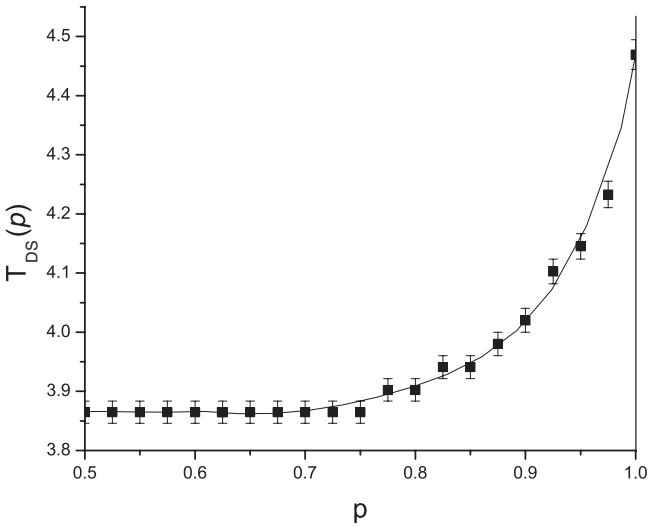

FIG. 7. Damage-spreading critical temperature $T_{\rm DS}(p)$ for a three-dimensional (3D) cubic lattice size $L = 32$. The error bars correspond mainly to the residual uncertainty in the extrapolation to the intersection with the β axis.

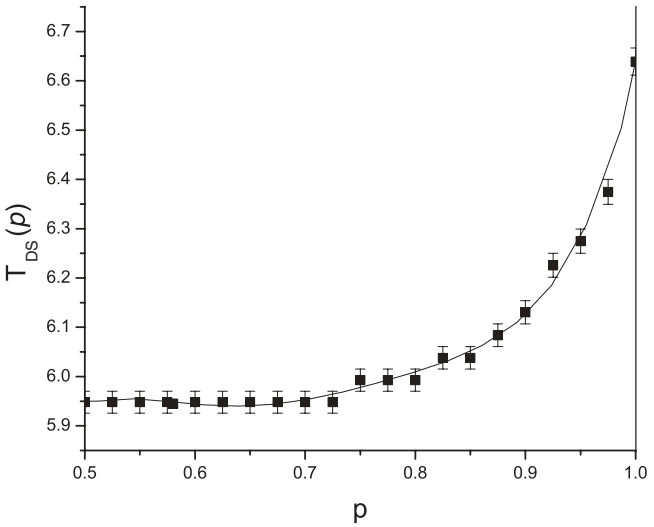

FIG. 8. Damage-spreading critical temperature $T_{\rm DS}(p)$ for a 4D cubic lattice size $L = 16$. The error bars correspond mainly to the residual uncertainty in the extrapolation to the intersection with the β axis.

L. One efficient method is to fit the envelope points, assuming that near $\beta_{\rm DS}$ the behavior follows $D(\beta) = A(\beta - \beta_{\rm DS})^B$ and adjusting B to obtain a straight line. We have also used a simple scaling formula $\beta_{\rm DS}(L) = \beta_{\rm DS} + CL^{-\lambda}$ to verify. Of course, a certain statistical uncertainty will enter depending on which L is included in the fitting process, which we take into account in the final error estimate.

The infinite-L damage-spreading temperatures $T_{\rm DS}(p_{\rm NL,FK})$ were estimated for the central values of $p_{\rm NL,FK}$ in the 3 dimensions: $T_{\rm DS}(p_{\rm NL,FK}) = 3.932(2)$ in dimension 3, $T_{\rm DS}(p_{\rm NL,FK}) = 6.057(10)$ in dimension 4, and $T_{\rm DS}(p_{\rm NL,FK}) = 8.13(1)$ in dimension 5. The observed ratios $T_{\rm FK}(p_{\rm NL,FK})/T_{\rm DS}(p_{\rm NL,FK})$ are equal to 1.0005(5), 1.022(2), and 1.036(10), respectively. In dimension 3, $T_{\rm DS}(p_{\rm NL,FK})$ is indistinguishable from $T_{\rm FK}(p_{\rm NL,FK})$, while in dimensions 4 and 5 the values appear tantalizingly close, but not identical. We have no explanation for the striking similarity between the two temperatures for the particular case of dimension 3. Adding a little more detail for this particular case, the individual $\beta_{\rm DS}(L)$ were estimated to an accuracy of ± 0.0001 for $L = 48,64$; $\pm 0.000\,25$ for $L = 32$; ± 0.0005 for $L = 16,20,24$; and ± 0.001 for $L = 12$. Using the exponent $\lambda = 2.05$ gives a projected $\beta_{\rm DS}$ that depends only to a very small degree on which L are included in the fit (though we always include $L = 48,64$). We receive a median value of $\beta_{\rm DS} = 0.254\,32$ and a standard deviation of $0.000\,15$, giving us $T_{\rm DS} = 3.932(2)$. Similar methods were used to estimate $T_{\rm DS}$ for the other dimensions.

As in dimension 2, the curve for $T_{\rm DS}(p)$ is almost flat over a wide range of p around $p = 1/2$ for dimensions 3 and 4 (Figs. 7 and 8) (the case of dimension 5 was not studied). These data are for fixed L ($L = 32$ and 16, respectively), so the $T_{\rm DS}(p)$ values are not quite equivalent to the values quoted for $T_{\rm DS}$ at $p_{\rm NL,FK}$. Judging from the behavior observed in dimension 2, it seems very plausible to assume that the ratio $T_{\rm FK}(p)/T_{\rm DS}(p)$ is always practically independent of p in the strong-disorder regime $1/2 < p < p_{\rm NL,FK}$.

It can be noted that numerical data for the time dependence of the autocorrelation function $q(t)$ at all temperatures in two-dimensional fully frustrated systems have been interpreted in terms of exponential relaxation with logarithmic corrections due to vortex-vortex interactions [37]. The results indicate that in these systems (which have well established FK and damage transitions) there is no dynamic critical temperature in the Ogielski sense [14].

VI. DAMAGE CLUSTERS

It is of interest to examine in some detail the damage clusters in dimension 2, where they can be readily visualized. Keeping $\beta > \beta_{\rm DS}$ and letting $t \to \infty$ (or at least allowing for equilibration), how does the damage actually spread? Note that we define a cluster as a connected component in the lattice induced by the damaged sites, i.e., a maximal set of damaged sites such that there is a lattice path (made up of horizontal and vertical steps) between each pair of sites. The sum of the individual cluster sizes is thus the damage without normalization, i.e., $L^d D(\beta)$. We have collected data on cluster sizes for $d = 2,3,4,5$. For $d = 2$ we have used only the square lattice, not the triangular lattice.

What we see in a square lattice snapshot at β near $\beta_{\rm DS}$ and at any arbitrary fixed time is not, as in the case for percolation (including FK percolation) or random graphs near p_c, the formation of a giant cluster, but rather a large number of very small clusters. At subsequent times the clusters evolve and flutter through the lattice. An example is shown in Fig. 9.

The measurements take place as above for the damage spreading; starting from random (infinite-temperature) spin configurations, at each time step we update L^d randomly selected sites and then search for all clusters and their sizes. On a measurement we collect the number of clusters, the average cluster size, the size of the largest cluster, and the size of a randomly selected cluster. As before, we collect 10^6 measurements from each sample after discarding between

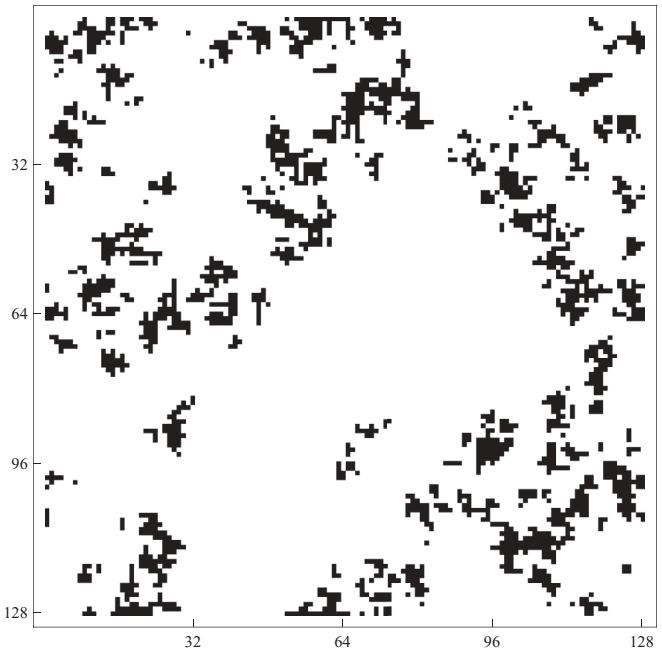

FIG. 9. Illustrative snapshot of an instantaneous damage site configuration for an $L = 128$ square lattice at $p = 0.75$ and temperature $T = 1.61$, just below the damage-spreading transition.

50 000 and 250 000 time steps (depending on L) to allow for equilibration of the damage spreading. We then average over the time steps to get the average for a particular sample. The data are then averaged over the samples; we have used only eight samples in each case for the cluster measurements (for the damage spreading we used between 8 and 128 samples, depending on lattice size). In all cases we have set $p = p_{\mathrm{NL,FK}}$.

First we discuss the expected number of clusters, which we denote $n_c(\beta,L)$. In Fig. 10 we plot $n_c(\beta,L)/L^3$ versus

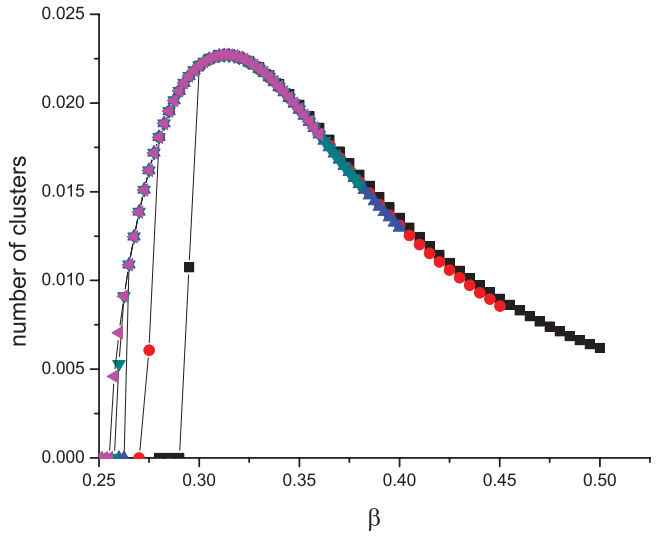

FIG. 10. (Color online) Number of clusters $n_c(\beta,L)$ on the 3D cubic lattice normalized by L^3 at $p = p_{\mathrm{NL,FK}}$. The sizes $L =$ 12, 16, 24, 32, and 48 are shown as black squares, red circles, blue triangles, green inverted triangles, and pink left-pointing triangles, respectively. The errors are smaller than the size of the points.

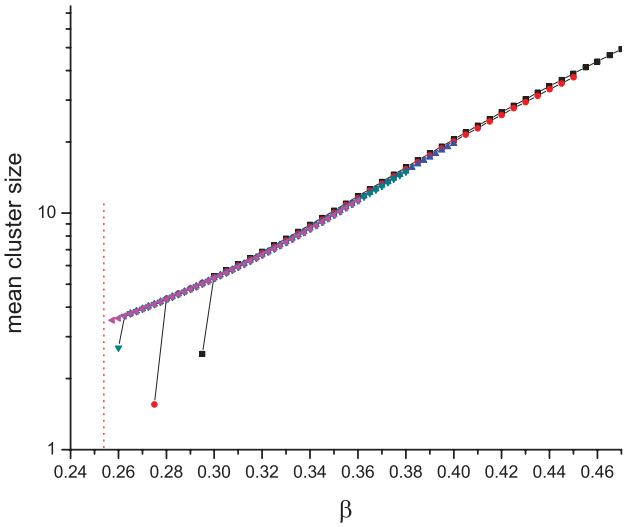

FIG. 11. (Color online) Mean cluster size $s(\beta,L)$ on the 3D cubic lattice at $p = p_{\mathrm{NL,FK}}$. The sizes $L = 12$, 16, 24, 32, and 48 are shown as black squares, red circles, blue triangles, green inverted triangles, and pink left-pointing triangles, respectively. The errors are smaller than the size of the points.

β for the simple cubic lattice. Equivalent behavior is found also for $d = 2,4,5$. Note that for the square lattice all lattice sizes agree on a global maximum probability located at $\beta_{\max} = 0.656(1)$, where $n_c(\beta_{\max},L) \sim 0.0130(1)\,L^2$. For $d = 3$ we obtain $\beta_{\max} = 0.313(1)$ and $n_c(\beta_{\max},L) \sim 0.0227(1)\,L^3$, for $d = 4$ we get $\beta_{\max} = 0.211(1)$ and $n_c(\beta_{\max},L) \sim 0.0200(1)\,L^4$, and for $d = 5$ we get $\beta_{\max} = 0.177(1)$ and $n_c(\beta_{\max},L) \sim 0.0308(1)\,L^5$. Thus the damage is always distributed over $O(L^d)$ clusters.

With so many clusters the average cluster at each time step must be rather small. We measure the number of damaged sites DL^d and the number of clusters n_c, giving us the mean cluster size at each time step. The normalized time average (and then the sample average, though the sample variation is very small) is then $s(\beta,L) = \langle DL^d/n_c \rangle$. In Fig. 11 we plot $s(\beta,L)$ versus β, again for $d = 3$. The curve clearly suggests a positive right limit at β_{DS}. To estimate this limit we fit a simple expression $a_0 + a_1 \exp(a_2\,\beta)$ to the points, resulting in $s(\beta_{\mathrm{DS}}) = \lim_{\beta\to\beta_{\mathrm{DS}}^+} \lim_{L\to\infty} s(\beta,L) = 3.46(1)$. We estimate the right limits corresponding to $d = 2$, 3, 4, and 5 to be, respectively, 9.00(2), 3.46(1), 2.76(1), and 1.95(1) sites at β_{DS}. One could alternatively define s as the average damage divided by the average number of clusters. This is not strictly the same as our present definition (mean ratio versus ratio of the means), but the difference is of course vanishingly small here. For example, the maximum in Fig. 10 at $\beta_{\max} = 0.313$ gives $n_c \sim 0.0227L^3$ and the number of damaged sites (see Fig. 6) is $0.139(1)L^3$. Hence the average cluster size is roughly 6.1, which matches Fig. 11.

We end this section with a final remark concerning the distribution of cluster sizes. At each time step we pick here one cluster uniformly at random and measure its size. In Fig. 12 we show a set of size distributions (or density functions) as ln Pr vs ln$s$ for a range of β for $d = 3$ and $L = 12$. They all have a high value at size 1 (many isolated sites) and then drop quickly. They can be expected to behave like this since the mean size

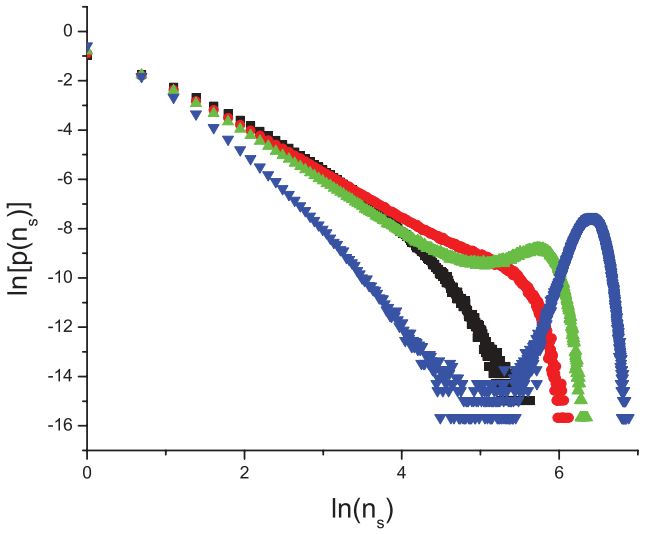

FIG. 12. (Color online) Distribution of cluster sizes on the 3D cubic lattice for $L = 12$ at inverse temperatures $\beta = 0.295$, 0.335, 0.370, and 0.500, shown as black squares, red circles, green triangles, and blue inverted triangles, respectively. The errors are the size of the points, except for very small p, where they can be judged by the scatter (note the logarithmic scales).

is between 4 and 70 in this temperature range. However, for $\beta > \beta_{\max}$ (or thereabout) the distributions show a second, and rather wide, maximum located in the neighborhood of the total damage $D(\beta, L)$. This can be understood as follows. Suppose for the sake of argument that the damaged sites are distributed at random in space. (This is only approximate as correlations between damage sites should be allowed for.) Then when $D(\beta)$ exceeds the site percolation concentration there will exist a single giant percolating cluster of damaged sites together with residual small clusters. As $D(\beta)$ increases further the percolating cluster will contain almost all the damaged sites. By this criterion the peak should appear in the distribution at $D(\beta) \sim 0.59$, 0.31, 0.20, and 0.14 in dimensions 2, 3, 4, and 5, respectively, which gives an indication in rough agreement with the data. Indeed, in the case of the square the peak never appears, which is consistent with the fact that $D(\beta)$ never approaches 0.59. For the dimensions where the peak does appear the global parameters, in particular $D(\beta)$, increase smoothly with β and show no sign of any critical behavior as the giant cluster forms.

VII. CONCLUSION

The exact values of the coordinates of the intersection point where the Fortuin-Kasteleyn transition line crosses the Nishimori line can be derived for an RBIM from the analytic condition that satisfied bonds are uncorrelated on the NL [21]. On any lattice this leads to the exact expressions $p_{\mathrm{NL,FK}} = (1 + P_c)/2$ and $T_{\mathrm{NL,FK}} = 2/\ln[(1 + P_c)/(1 - P_c)]$ [19,20], where P_c is the standard random-bond percolation concentration for the particular lattice. For lattices in dimension 2 (and probably in higher dimensions also) the uncorrelated bond condition remains a very good approximation at the FK transition temperature over a wide strong-disorder region spanning $p = 1/2$.

In pure ferromagnets $T_{\mathrm{FK}}(p = 1) = T_{\mathrm{DS}}(p = 1) = T_c(p = 1)$. The conjectured equivalence for the RBIM between the FK transition temperature and the heat-bath damage-spreading temperature, $T_{\mathrm{FK}}(p) \sim T_{\mathrm{DS}}(p)$ [7,19,20], separating an exponential from a chaotic dynamic regime has been tested at $p = p_{\mathrm{NL,FK}}$ on simple cubic lattices in dimensions 2–5. It holds to within 0.1% in dimension 3, to within 2% in dimension 4, and to 3% in dimension 5. The equivalence appears always to be a good approximation. We have no explanation to propose for the quasiequality in the case of dimension 3. For the square and triangle lattices the difference is larger: 5% and 16%, respectively.

The FK transition in the strong-disorder regime close to $p = 1/2$ can thus be said to be well understood. However, the basic physical condition determining the damage-spreading transition temperature, which plays an important role in limiting perfect equilibration in RBIMs, and its proximity to the FK transition remains unclear.

ACKNOWLEDGMENTS

We are very grateful for enlightening remarks by H. Nishimori, C. Yamaguchi, R. Ziff, and W. Krauth. The computations were performed on resources provided by the Swedish National Infrastructure for Computing (SNIC) at High Performance Computing Center North (HPC2N).

[1] R. B. Griffiths, Phys. Rev. Lett. **23**, 17 (1969).
[2] Y. Matsuda, H. Nishimori, and K. Hukushima, J. Phys. A: Math. Theor. **41**, 324012 (2008).
[3] H. Nishimori, Prog. Theor. Phys. **66**, 1169 (1981).
[4] C. M. Fortuin and P. W. Kasteleyn, Physica **57**, 536 (1972).
[5] A. Coniglio and W. Klein, J. Phys. A **13**, 2775 (1980).
[6] A. Coniglio, F. di Liberto, G. Monroy, and F. Peruggi, Phys. Rev. B **44**, 12605 (1991).
[7] L. de Arcangelis, A. Coniglio, and F. Peruggi, Europhys. Lett. **14**, 515 (1991).
[8] V. Cataudella, Physica A **183**, 249 (1991).
[9] M. Zhang and C. Z. Yang, Europhys. Lett. **22**, 505 (1993).
[10] B. Derrida and G. Weisbuch, Europhys. Lett. **4**, 657 (1987).
[11] B. Derrida, Phys. Rep. **184**, 207 (1989).
[12] L. de Arcangelis, A. Coniglio, and H. Herrmann, Europhys. Lett. **9**, 749 (1989).
[13] I. A. Campbell and L. de Arcangelis, Physica A **178**, 29 (1991).
[14] A. T. Ogielski, Phys. Rev. B **32**, 7384 (1985).
[15] R. H. Swendsen and J.-S. Wang, Phys. Rev. Lett. **58**, 86 (1987).
[16] U. Wolff, Phys. Rev. Lett. **62**, 361 (1989).
[17] J. Propp and D. Wilson, Random Struct. Algor. **9**, 223 (1996).
[18] E. P. Bernard, C. Chanal, and W. Krauth, Europhys. Lett. **92**, 60004 (2010).
[19] I. A. Campbell and L. Bernardi, Phys. Rev. B **50**, 12643 (1994).

[20] C. Yamaguchi, arXiv:1004.0654.
[21] H. Nishimori, Prog. Theor. Phys. **76**, 305 (1986).
[22] H. Nishimori, *Statistical Physics of Spin Glasses and Information Processing: An Introduction* (Oxford University Press, Oxford, 2001), p. 51.
[23] S. Prakash, A. Coniglio, and H. E. Stanley, Phys. Rev. E **49**, 2742 (1994).
[24] V. Cataudella, A. Coniglio, L. de Arcangelis, and F. di Liberto, Physica A **192**, 167 (1993).
[25] H. Imaoka, H. Ikeda, and Y. Kasai, Physica A **246**, 18 (1997).
[26] C. Chanal and W. Krauth, Phys. Rev. Lett. **100**, 060601 (2008).
[27] C. Chanal and W. Krauth, Phys. Rev. E **81**, 016705 (2010).
[28] F. D. Nobre, Phys. Rev. E **64**, 046108 (2001).
[29] C. Wang, J. Harrington, and J. Preskill, Ann. Phys. **303**, 31 (2003).
[30] C. Amoruso and A. K. Hartmann, Phys. Rev. B **70**, 134425 (2004).
[31] F. Parisen Toldin *et al*., J. Stat. Phys. **135**, 1039 (2009).
[32] C. K. Thomas and H. G. Katzgraber, Phys. Rev. E **84**, 040101(R) (2011).
[33] R. Häggkvist and P. H. Lundow, J. Stat. Phys. **108**, 429 (2002).
[34] M. Hasenbusch, F. Parisen Toldin, A. Pelissetto, and E. Vicari, Phys. Rev. E **77**, 051115 (2008).
[35] C. D. Lorenz and R. M. Ziff, Phys. Rev. E **57**, 230 (1998).
[36] S. M. Dammer and H. Hinrichsen, J. Stat. Mech. (2004) P07011.
[37] J.-C. Walter and C. Chatelain, J. Stat. Mech. (2012) P02010.